



*Supplement of*

**Extension, development, and evaluation of the representation of the OH-initiated dimethyl sulfide (DMS) oxidation mechanism in the Master Chemical Mechanism (MCM) v3.3.1 framework**

**Lorrie Simone Denise Jacob et al.**

*Correspondence to:* Lorrie Simone Denise Jacob ([lj384@cam.ac.uk](mailto:lj384@cam.ac.uk)) and Alexander Thomas Archibald ([ata27@cam.ac.uk](mailto:ata27@cam.ac.uk))

The copyright of individual parts of the supplement might differ from the article licence.

## **S1 Reactions added and adjusted from the MCM in the Jernigan, Shen and Ye mechanisms**

The following tables provide the additions and adjustments to the MCM v3.3.1 DMS mechanism to make the Jernigan, Shen and Ye mechanisms (Jernigan et al., 2022; Shen et al., 2022; Ye et al., 2022) used in this work. The references for each of the reactions come directly from the papers themselves, and only changes to the sulfur reactions presented in the papers were included in these mechanisms. The ‘adjusted’ reactions refer to adjustments of rate constants or products of the reactions in the MCM.

**Table S1: The reactions added to the base MCM mechanism to make the Ye et al. (2022) mechanism**

Reaction		Rate constant	Source	
1	$\text{CH}_3\text{SCH}_2\text{O}_2$	$= \text{HOCH}_2\text{SCH}_2\text{O}_2$	$9.00 \times 10^{-2}$	Ye et al. (2021)
2	$\text{HOCH}_2\text{SCH}_2\text{O}_2$	$= \text{HPMTF} + \text{OH}$	$5.8 \times 10^{11} \times e^{-10155/T+1080200/T^2}$	Wu et al. (2015)
3	$\text{HOCH}_2\text{SCH}_2\text{O}_2 + \text{NO}$	$= \text{HOCH}_2\text{SCH}_2\text{O} + \text{NO}_2$	$4.9 \times 10^{-12} \times e^{260/T}$	MCM v3.3.1 (SAR)
4	$\text{HOCH}_2\text{SCH}_2\text{O}_2 + \text{HO}_2$	$= \text{HOCH}_2\text{SCH}_2\text{OOH}$	$1.13 \times 10^{-13} \times e^{1300/T}$	MCM v3.3.1 (SAR)
5	$\text{HOCH}_2\text{SCH}_2\text{O}$	$= \text{HOCH}_2\text{S} + \text{HCHO}$	$1 \times 10^6$	MCM v3.3.1 (SAR)
6	$\text{HPMTF} + \text{OH}$	$= \text{HOCH}_2\text{SCO}$	$1 \times 10^{-11}$	Vermeuel et al. (2020)
7	$\text{HOCH}_2\text{SCO}$	$= \text{HOCH}_2\text{S} + \text{CO}$	$9.2 \times 10^9 \times e^{-505.4/T}$	Wu et al. (2015)
8	$\text{HOCH}_2\text{SCO}$	$= \text{OH} + \text{HCHO} + \text{OCS}$	$1.6 \times 10^7 \times e^{-1468.6/T}$	Wu et al. (2015)
9	$\text{HOCH}_2\text{S} + \text{NO}_2$	$= \text{HOCH}_2\text{SO} + \text{NO}$	$6.0 \times 10^{-11} \times e^{240/T}$	MCM v3.3.1 (SAR)
10	$\text{HOCH}_2\text{S} + \text{O}_3$	$= \text{HOCH}_2\text{SO}$	$1.15 \times 10^{-12} \times e^{430/T}$	MCM v3.3.1 (SAR)
11	$\text{HOCH}_2\text{SO} + \text{O}_3$	$= \text{SO}_2 + \text{HCHO} + \text{OH}$	$4.0 \times 10^{-13}$	MCM v3.3.1 (SAR)
12	$\text{HOCH}_2\text{SO} + \text{NO}_2$	$= \text{SO}_2 + \text{HCHO} + \text{OH} + \text{NO}$	$1.2 \times 10^{-11}$	MCM v3.3.1 (SAR)

**Table S2: The reactions added to the base MCM mechanism in the Jernigan et al. (2022) mechanism. These reactions and their rate constants were taken from the equation and README files included in the archive containing the data for their paper.**

Reaction	Rate constant	Source
1 $\text{CH}_3\text{SCH}_2\text{O}_2 = \text{HPMTF} + \text{OH}$	$1.00 \times 10^{-1}$	Jernigan et al. (2022)
2 $\text{HPMTF} + \text{OH} = \text{OCS}$	$1.4 \times 10^{-11} \times 0.14$	Jernigan et al. (2022)
3 $\text{HPMTF} + \text{OH} = \text{SO}_2 + \text{CO}$	$1.4 \times 10^{-11} \times 0.86$	Jernigan et al. (2022)
4 $\text{OCS} + \text{OH} = \text{SO}_2$	$1.1 \times 10^{-13} \times e^{-1200/T}$	Atkinson et al. (2004)
5 $\text{DMSO} + \text{OH} = \text{DMSO}_2$	$6.10 \times 10^{-12} \times e^{800/T} \times 0.1$	MCM v3.3.1 with Jernigan et al. (2022) branching ratio

**Table S3: The reactions adjusted from the base MCM mechanism in the Jernigan et al. (2022) mechanism. These reactions and their rate constants were taken from the equation and README files included in the archive containing the data for their paper.**

Reaction	Rate constant	Source
1 $\text{CH}_3\text{SCH}_2\text{O}_2 = \text{CH}_3\text{SCH}_2\text{O}$	$10 \times 10^{-12} \times [\text{RO}_2] \times 0.8$	based off Burkholder et al. (2019) self-reaction
2 $\text{CH}_3\text{SCH}_2\text{O}_2 = \text{CH}_3\text{SCH}_2\text{OH}$	$10 \times 10^{-12} \times [\text{RO}_2] \times 0.1$	based off Burkholder et al. (2019) self-reaction
3 $\text{CH}_3\text{SCH}_2\text{O}_2 = \text{CH}_3\text{SCHO}$	$10 \times 10^{-12} \times [\text{RO}_2] \times 0.1$	based off Burkholder et al. (2019) self-reaction
4 $\text{DMSO} + \text{OH} = \text{MSIA} + \text{CH}_3\text{O}_2$	$6.10 \times 10^{-12} \times e^{800/T} \times 0.9$	MCM v3.3.1 with Jernigan et al. (2022) branching ratio

**Table S4: The reactions added to the base MCM mechanism in the Shen et al. (2022) mechanism.**

Reaction	Rate constant	Source
1 $\text{CH}_3\text{S}(\text{OH})\text{CH}_3$	$\text{DMS} + \text{OH}$	Lucas and Prinn (2002)
2 $\text{CH}_3\text{S}(\text{OH})\text{CH}_3$	$\text{HODMSO}_2$	Sander et al. (2011)
3 $\text{CH}_3\text{S}(\text{OH})\text{CH}_3$	$\text{CH}_3\text{SOH} + \text{CH}_3\text{O}_2$	MCM v3.3.1
4 $\text{DMSO} + \text{OH}$	$\text{DMSO}_2$	Shen et al. (2022)
5 $\text{DMSO} + \text{NO}_3$	$\text{DMSO}_2 + \text{NO}_2$	Sander et al. (2011)
6 $\text{CH}_3\text{SOH} + \text{OH}$	$\text{CH}_3\text{SO}$	MCM v3.3.1
7 $\text{MSIA} + \text{NO}_3$	$\text{CH}_3\text{SO}_2 + \text{HNO}_3$	Yin et al. (1990)
8 $\text{CH}_3\text{SOO} + \text{HO}_2$	$\text{CH}_3\text{SOOH}$	MCM v3.3.1
9 $\text{CH}_3\text{SOO}$	$\text{CH}_3\text{SO}_2$	Hoffmann et al. (2016)
10 $\text{CH}_3\text{SO}_2 + \text{OH}$	$\text{MSA}$	Yin et al. (1990)
11 $\text{CH}_3\text{SO}_2 + \text{NO}_2$	$\text{CH}_3\text{SO}_3 + \text{NO}$	Sander et al. (2011)
12 $\text{CH}_3\text{SCH}_2\text{O}_2$	$\text{HOOCH}_2\text{SCH}_2\text{O}_2$	Veres et al. (2020); Berndt et al. (2019)
13 $\text{HOOCH}_2\text{SCH}_2\text{O}_2$	$\text{HPMTF} + \text{OH}$	Veres et al. (2020)
14 $\text{HOOCH}_2\text{SCH}_2\text{O}_2 + \text{NO}$	$\text{HOOCH}_2\text{SCH}_2\text{O} + \text{NO}_2$	Wu et al. (2015)
15 $\text{HOOCH}_2\text{SCH}_2\text{O}$	$\text{HOOCH}_2\text{S} + \text{HCHO}$	Wu et al. (2015)
16 $\text{HOOCH}_2\text{SCH}_2\text{O}_2 + \text{HO}_2$	$\text{HOOCH}_2\text{SCH}_2\text{OOH}$	Wu et al. (2015)
17 $\text{HPMTF} + \text{OH}$	$\text{HOOCH}_2\text{SCO}$	Wu et al. (2015)
18 $\text{HOOCH}_2\text{SCO}$	$\text{HOOCH}_2\text{S} + \text{CO}$	Wu et al. (2015)
19 $\text{HOOCH}_2\text{SCO}$	$\text{OH} + \text{HCHO} + \text{OCS}$	Wu et al. (2015)
20 $\text{HOOCH}_2\text{S} + \text{O}_3$	$\text{HOOCH}_2\text{SO}$	Wu et al. (2015)
21 $\text{HOOCH}_2\text{S} + \text{NO}_2$	$\text{HOOCH}_2\text{SO} + \text{NO}$	Wu et al. (2015)
22 $\text{HOOCH}_2\text{SO} + \text{O}_3$	$\text{SO}_2 + \text{HCHO} + \text{OH}$	Wu et al. (2015)
23 $\text{HOOCH}_2\text{SO} + \text{NO}_2$	$\text{SO}_2 + \text{HCHO} + \text{OH} + \text{NO}$	Wu et al. (2015)
24 $\text{MSIA} + \text{O}_3$	$\text{MSA}$	Lucas and Prinn (2002)
25 $\text{CH}_3\text{SOH} + \text{O}_3$	$\text{CH}_3\text{O}_2 + \text{HO}_2 + \text{SO}_2$	Berndt et al. (2020)

**Rate constants:**  $K_f = 1.7 \times 10^{-42} \times [\text{O}_2] \times e^{7810/T} / (1 + 5.5 \times 10^{-31} \times [\text{O}_2] \times e^{7460/T})$ ,  $K_{eq} = (8.3 \times 10^{-29} \times T \times e^{5136/T})$ ,  $\text{HPTMF}_{\text{isom1}} = 2.2 \times 10^{11} \times e^{-9.8 \times 10^3/T} \times e^{1.0 \times 10^8/T^3} \times 5$ ,  $\text{HPTMF}_{\text{isom2}} = 6.1 \times 10^{11} \times e^{-9.5 \times 10^3/T+1.1 \times 10^8/T^3}$

**Table S5: The reactions adjusted from the base MCM mechanism in the Shen et al. (2022) mechanism**

Reaction	Rate constant	Source
1 DMS + OH = CH <sub>3</sub> S(OH)CH <sub>3</sub>	$9.5 \times 10^{-39} \times [\text{O}_2] \times e^{5270/T} / (1 + 7.5 \times 10^{-29} \times [\text{O}_2] \times e^{5610/T})$	MCM v3.3.1
2 MSIA + OH = CH <sub>3</sub> SO <sub>2</sub>	$1.60 \times 10^{-11}$	Yin et al. (1990)
3 CH <sub>3</sub> SO + O <sub>3</sub> = CH <sub>3</sub> O <sub>2</sub> + SO <sub>2</sub>	$6.00 \times 10^{-13}$	Berndt et al. (2020)
4 CH <sub>3</sub> SO <sub>2</sub> = CH <sub>3</sub> O <sub>2</sub> + SO <sub>2</sub>	$8.80 \times 10^{14} \times e^{-9673/T}$	Wu et al. (2015)

## S2 Modelling the Albu *et al.* experiment

10 As the Albu *et al.* (2008) experiment was not modelled in their paper, a different approach was taken to model their experiment. The input parameters for the model were taken from the experimental conditions described in the paper, however, the photolysis rate was not given and needed to be found through the best fit of the experimental data. In the case of Albu *et al.* (2008), ultraviolet (UV) lamps with a peak wavelength of 254 nm were used to photolyse the  $\text{H}_2\text{O}_2$  in the reaction chamber into two OH radicals. The photolysis rate constant ( $J$ ) of  $\text{H}_2\text{O}_2$  was adjusted until a good fit was found with the loss of DMS  
15 measured in the experiment. The photolysis rate found to replicate the Albu *et al.* (2008) experiment was  $1.4 \times 10^{-4} \text{ s}^{-1}$ , and the photolysis of products that absorbed at 254 nm (such as methyl hydroperoxide,  $\text{CH}_3\text{OOH}$  and methyl thioformate, MTF) were also included.

Figure S1 shows the loss of DMS observed by Albu *et al.* (2008) compared to the box model runs. The fit initially deviates from the experimental values. This deviation could be partly due to the experimental data being extracted from figures of Albu  
20 *et al.* (2008) using Webdigitizer. The digitisation of data can lead to some inconsistencies with the original data, such as the initial concentration not starting at the zeroth time step in Figure S1.

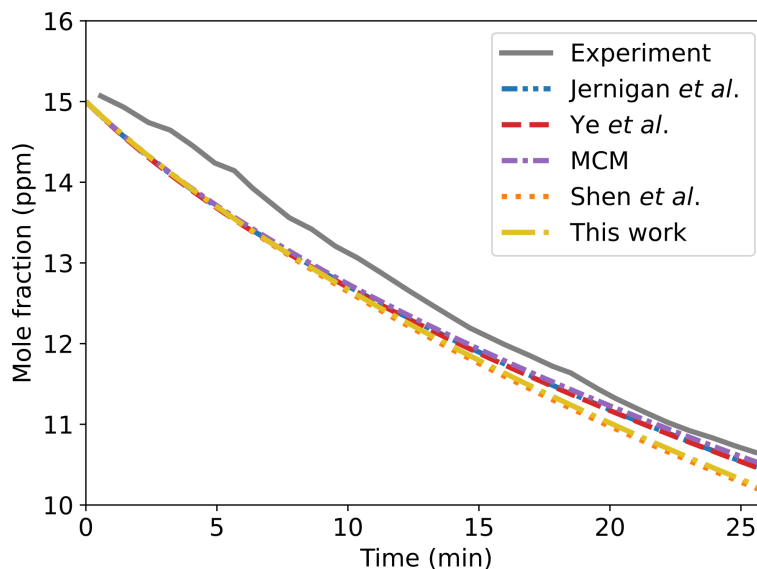


**Figure S1.** The measured DMS concentration in the Albu *et al.* (2008) experiment, compared to the model runs using different mechanisms (Jernigan, Ye, Shen, MCM, and the mechanism from this work). The photolysis rate of  $\text{H}_2\text{O}_2$  was set so that the modelled loss of DMS matched the concentration measured.

### S3 Modelling the Ye *et al.* experiment 1

The modelling of Ye *et al.* (2022) experiment 1 was initially replicated with the same input parameters as used in the paper, as shown in Figure 2 of the main text. However, for this study, one parameter was changed: the initial concentration of NO<sub>2</sub>. In the modelling of experiment 1, the authors set the initial NO<sub>2</sub> mole fraction to zero, although it was measured to be 88 ppb at the start of the experiment. Figure S2 shows that changing the input NO<sub>2</sub> mole fraction to 88 ppb results in fewer OH radicals reacting with DMS in the model, which results in 26% less DMS reacting using the same mechanism used in the paper (Ye mechanism) and 32% less DMS reacted in the model compared to the experiment. The figure shows the raw DMS measured in the experiment, uncorrected for dilution, alongside the modelling from the Ye mechanism and the mechanism developed in this work (all of which include the loss of DMS from dilution). The pink dashed line represents the modelling conducted by Ye *et al.* (2022) in their paper, which was shown in Figure 2 of the main text. The red dashed line uses the same mechanism, however, it includes the initial 88 ppb of NO<sub>2</sub>; this modelling is used to represent the Ye mechanism in the rest of the paper.

The subsequent deviation between the model output and the measured loss of DMS is later explained as being due to the CH<sub>3</sub>SO<sub>3</sub> radicals formed reacting with DMS to form methane sulfonic acid (CH<sub>3</sub>SO<sub>3</sub>H, MSA) and a CH<sub>3</sub>SCH<sub>2</sub> radical, a reaction which was not included in the mechanism used by Ye *et al.* (2022) (this is discussed further in Section 5 of the main text). Our mechanism (yellow dot-dashed line), with the inclusion of this reaction, is able to replicate the measured DMS with the initial NO<sub>2</sub> mole fraction of 88 ppb.

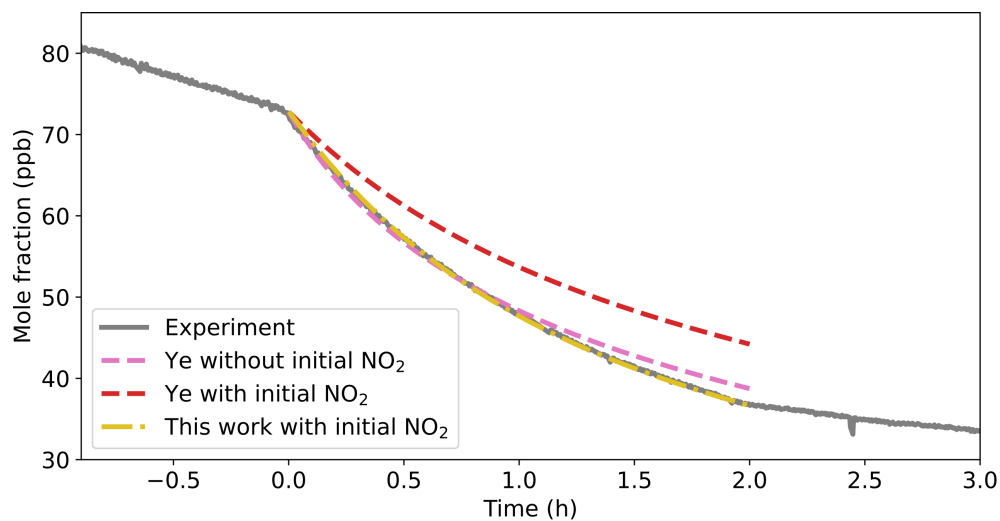


**Figure S2.** The raw measured DMS (grey solid line) from Ye *et al.* (2022) experiment 1, compared to the modelling of the Ye mechanism and the mechanism from this work (red dashed line and yellow dot-dashed line, respectively). In addition, the original modelling from Ye *et al.* (2022) is included (pink dashed line).



## S4 Modelling of the different experiments

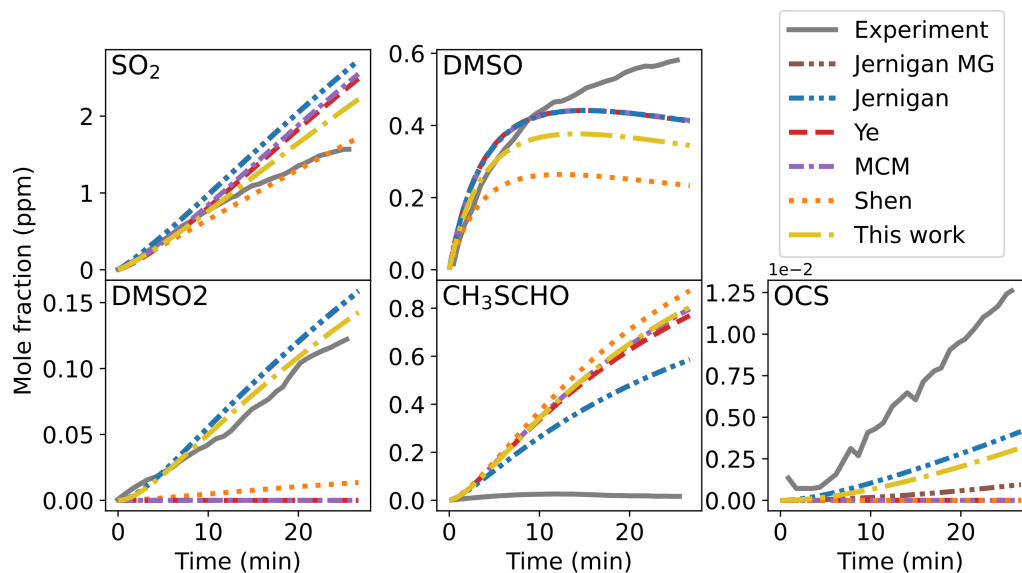


**Figure S3.** The products measured in the Albu et al. (2008) experiment, compared to the modelling results from the Jernigan, Ye, MCM and Shen mechanisms, along with the mechanism developed in this work, and the Jernigan multi-generational mechanism (Jernigan MG). Note that Jernigan MG can only be seen when it deviates from the Jernigan mechanism (first-generational mechanism).

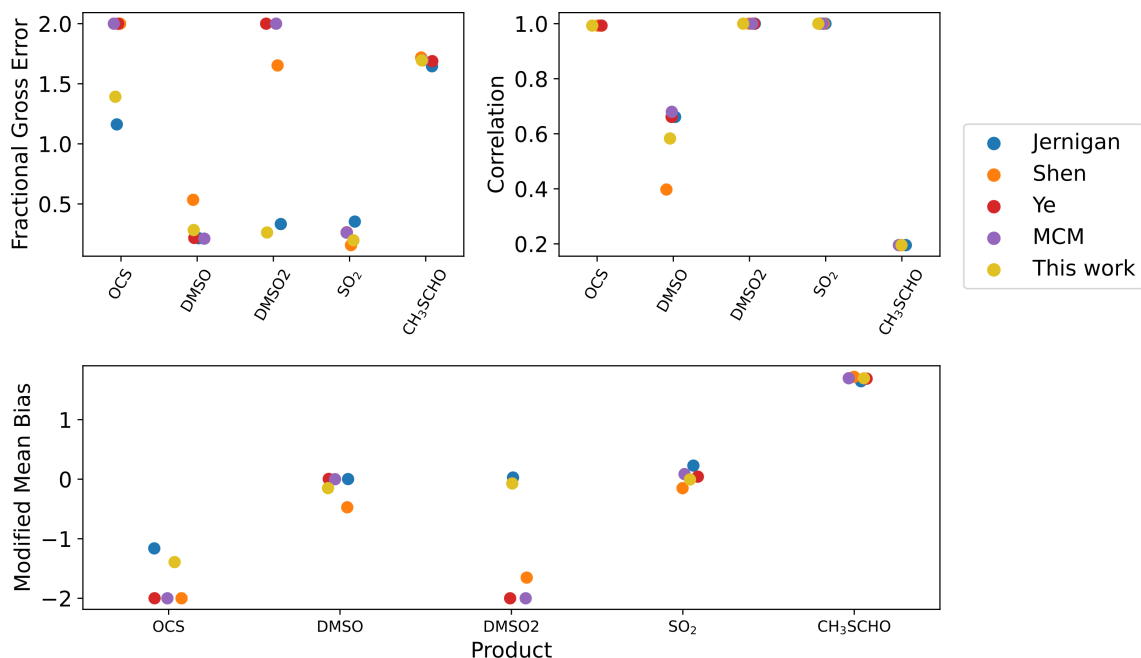


**Figure S4.** The fractional gross error, correlation coefficient and modified mean bias of the mechanisms for all species measured in the Albu et al. (2008) experiment.

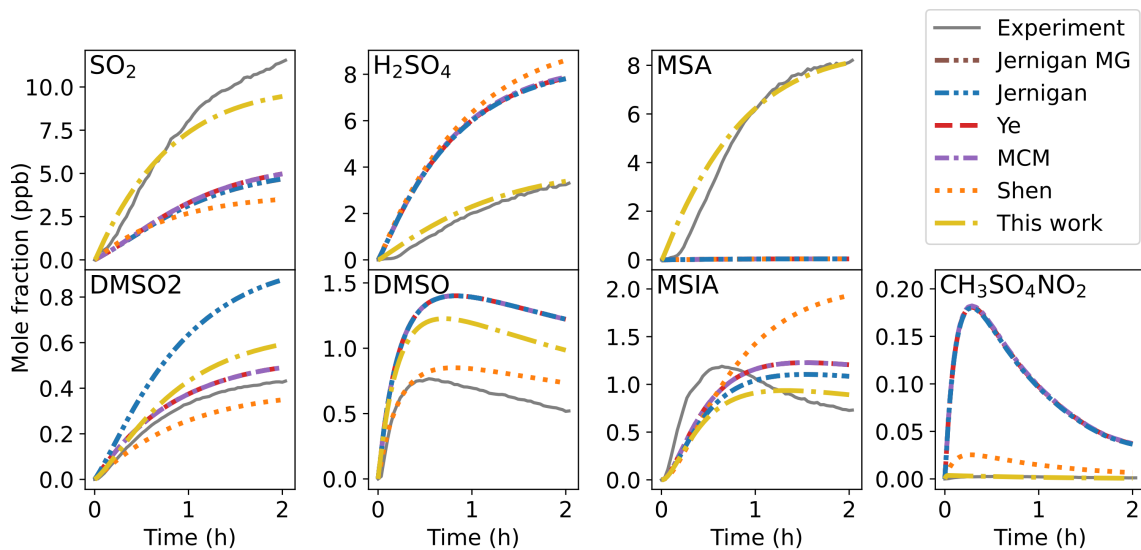


**Figure S5.** The products measured in the Ye et al. (2022) experiment 1, compared to the modelling results from the Jernigan, Ye, MCM and Shen mechanisms, along with the mechanism developed in this work, and the Jernigan multi-generational mechanism (Jernigan MG). Note that Jernigan MG can only be seen when it deviates from the Jernigan mechanism (first-generational mechanism). Additionally, the experimental DMSO<sub>2</sub> represents the product C<sub>2</sub>H<sub>6</sub>SO<sub>2</sub> measured by Ye et al. (2022), which may also include CH<sub>3</sub>SCH<sub>2</sub>OOH.

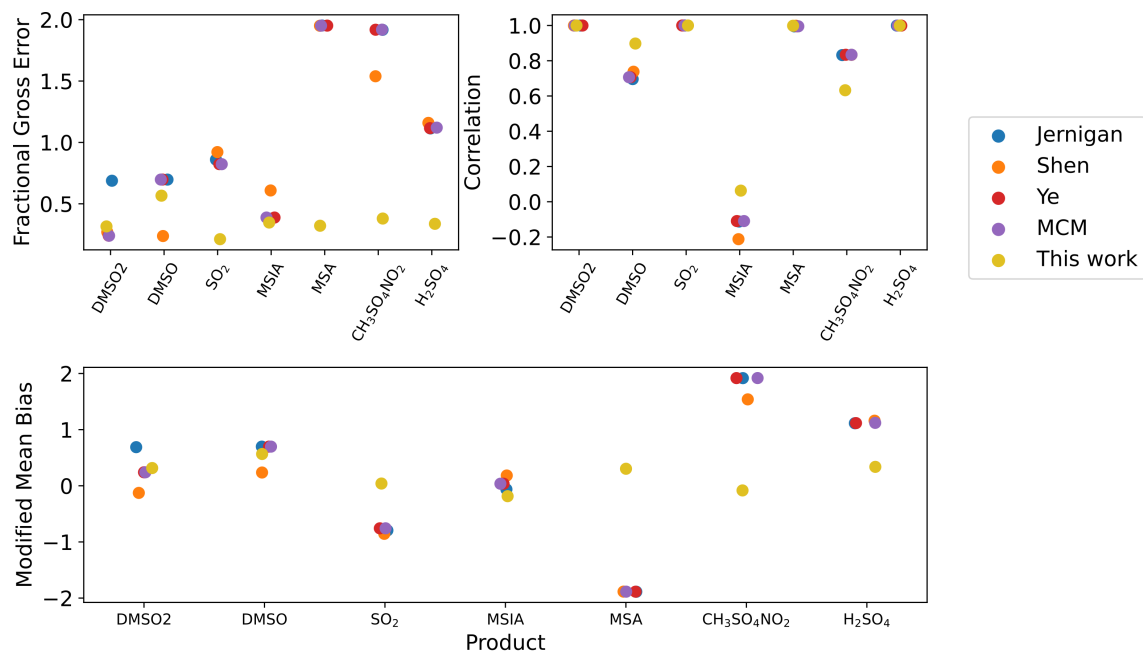


**Figure S6.** The fractional gross error, correlation coefficient and modified mean bias of the mechanisms for all species measured in the Ye et al. (2022) experiment 1. Note that the observed DMSO<sub>2</sub> represents the product C<sub>2</sub>H<sub>6</sub>SO<sub>2</sub> measured by Ye et al. (2022), which may also include CH<sub>3</sub>SCH<sub>2</sub>OOH.

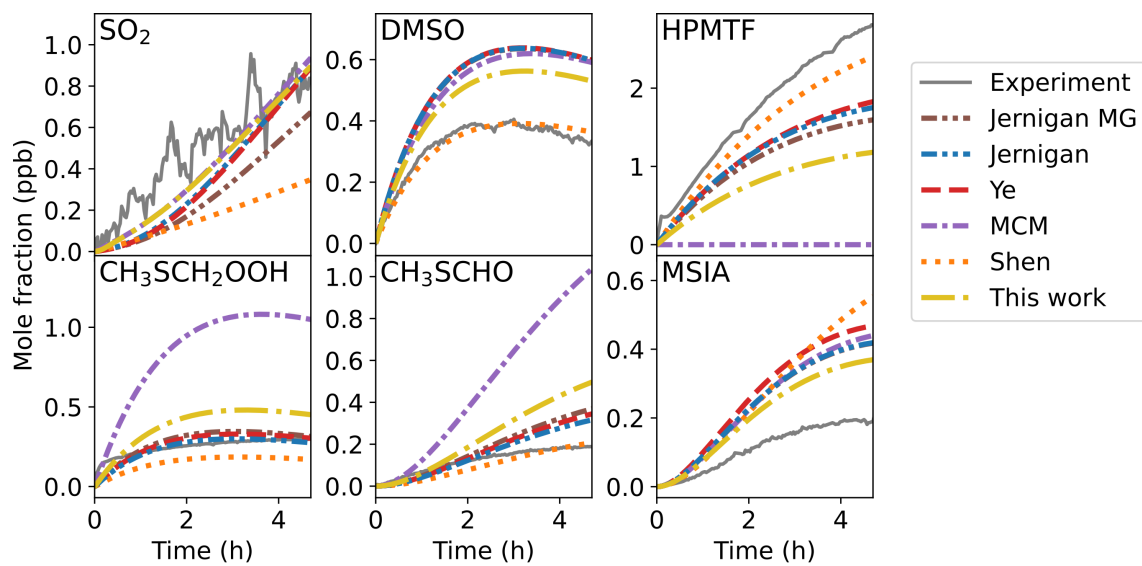


**Figure S7.** The products measured in the Ye et al. (2022) experiment 2a, compared to the modelling results from the Jernigan, Ye, MCM and Shen mechanisms, along with the mechanism developed in this work, and the Jernigan multi-generational mechanism (Jernigan MG). Note that Jernigan MG can only be seen when it deviates from the Jernigan mechanism (first-generational mechanism). Additionally, the experimental  $\text{CH}_3\text{SCH}_2\text{OOH}$  represents the product  $\text{C}_2\text{H}_6\text{SO}_2$  measured by Ye et al. (2022), which may also include  $\text{DMSO}_2$ .

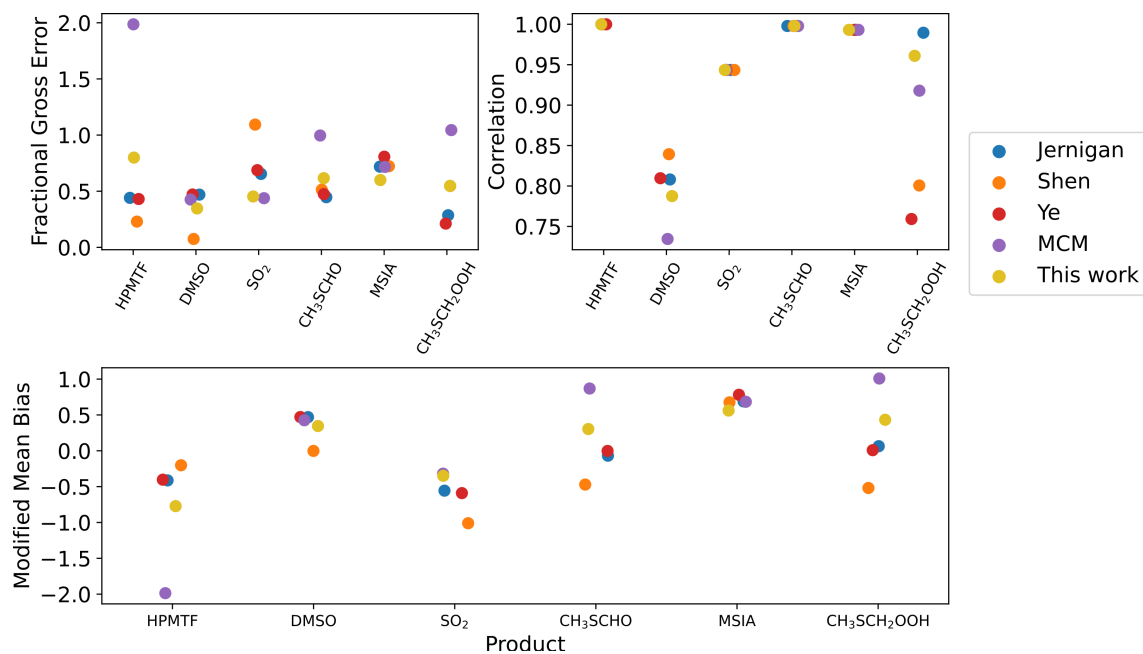


**Figure S8.** The fractional gross error, correlation coefficient and modified mean bias of the mechanisms for all species measured in the Ye et al. (2022) experiment 2a. Note that the observed CH<sub>3</sub>SCH<sub>2</sub>OOH represents the product C<sub>2</sub>H<sub>6</sub>SO<sub>2</sub> measured by Ye et al. (2022), which may also include DMSO<sub>2</sub>.

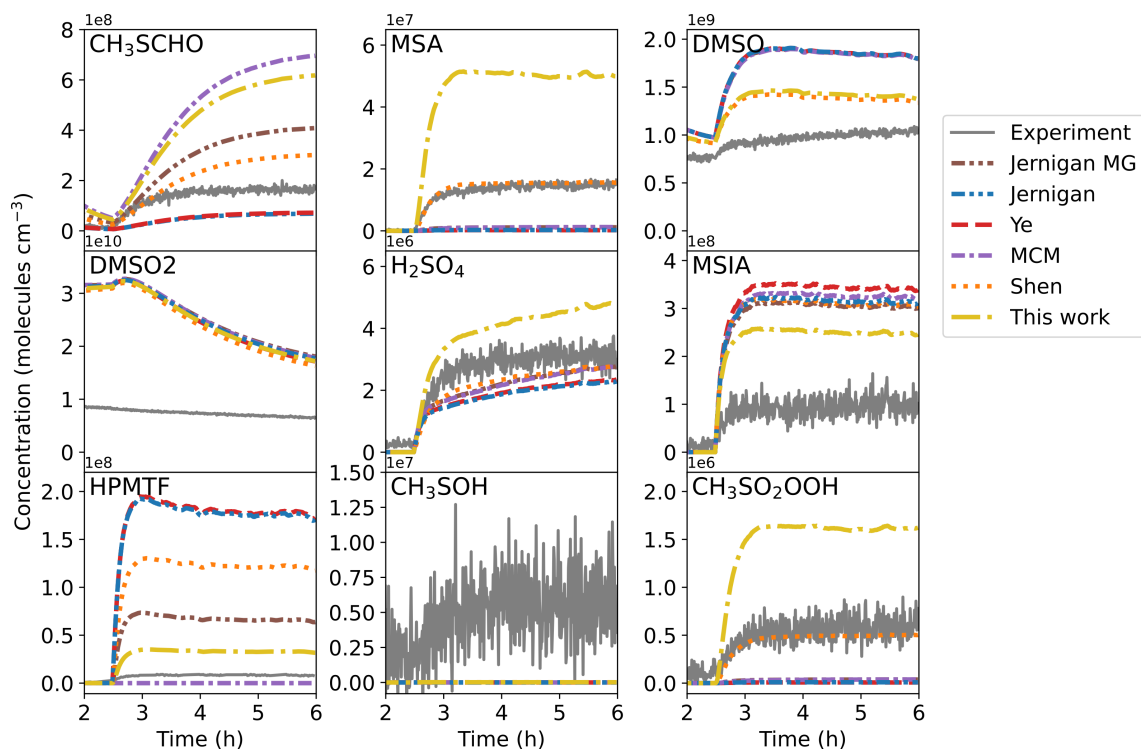


**Figure S9.** The products measured in the Shen et al. (2022) experiment, compared to the modelling results from the Jernigan, Ye, MCM and Shen mechanisms, along with the mechanism developed in this work, and the Jernigan multi-generational mechanism (Jernigan MG). Note that Jernigan MG can only be seen when it deviates from the Jernigan mechanism (first-generational mechanism).

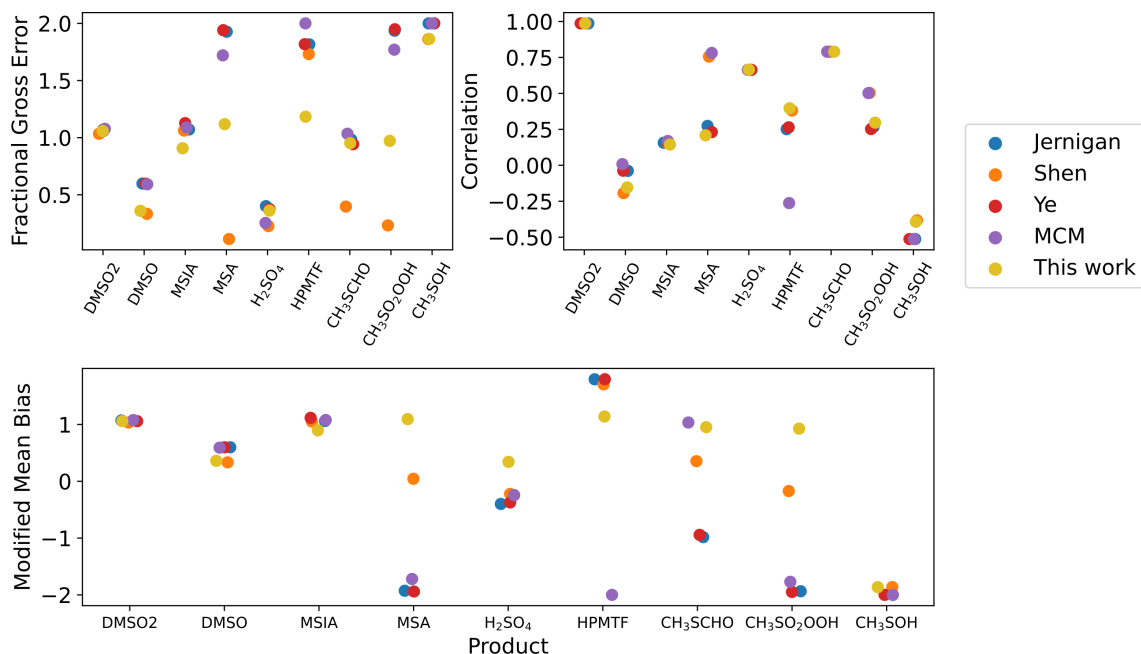


**Figure S10.** The fractional gross error, correlation coefficient and modified mean bias of the mechanisms for all species measured in the Shen et al. (2022) experiment.

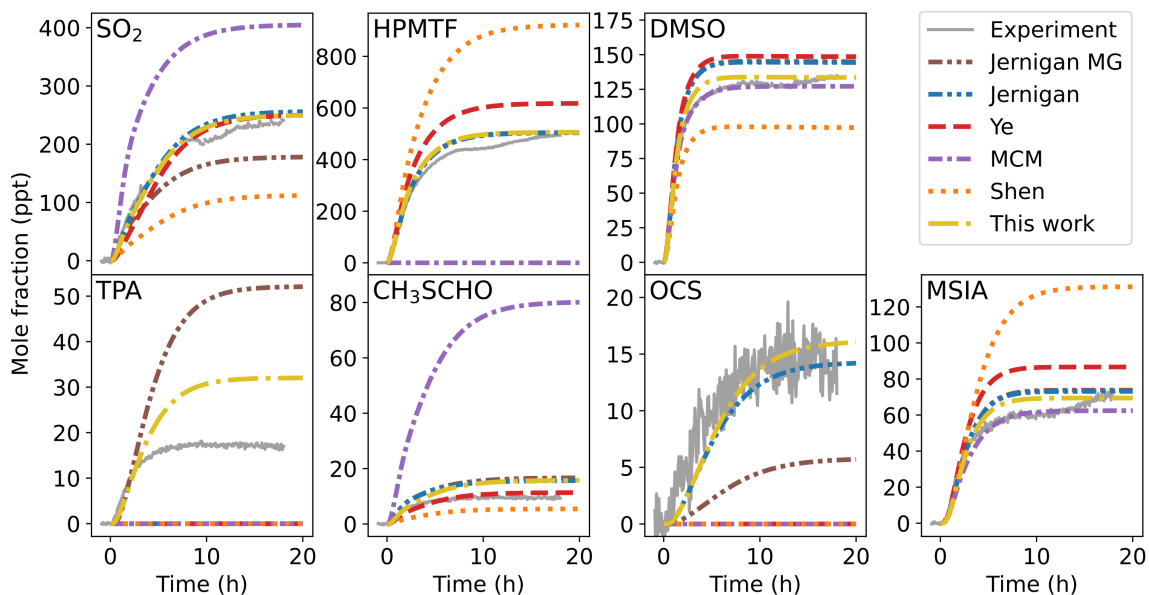


**Figure S11.** The products measured in the Jernigan et al. (2022) experiment, compared to the modelling results from the Jernigan, Ye, MCM and Shen mechanisms, along with the mechanism developed in this work, and the Jernigan multi-generational mechanism (Jernigan MG). Note that Jernigan MG can only be seen when it deviates from the Jernigan mechanism (first-generational mechanism).

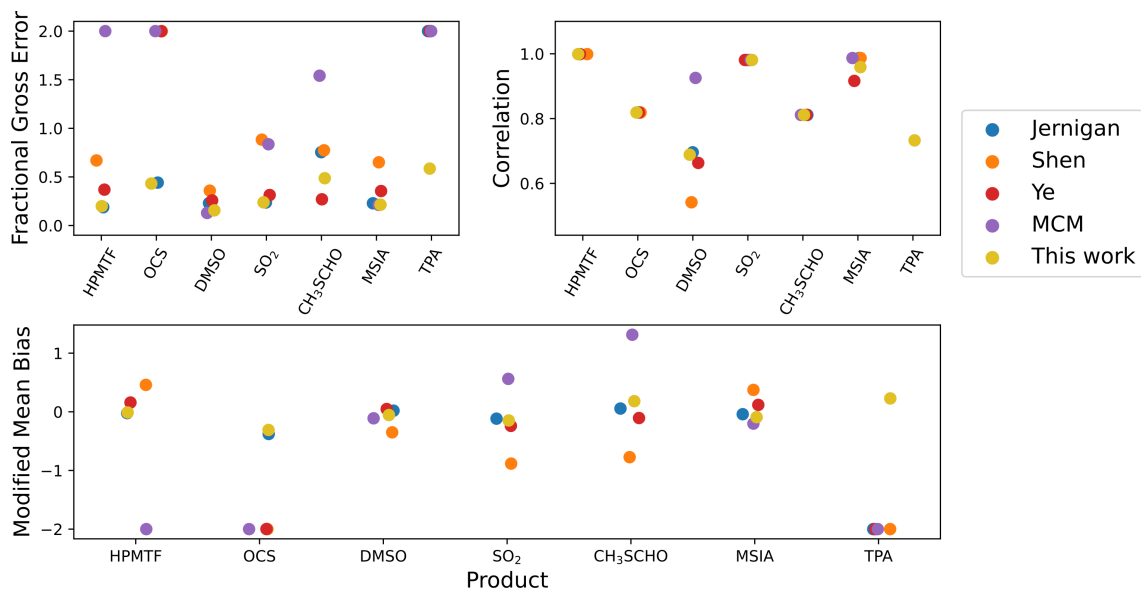


**Figure S12.** The fractional gross error, correlation coefficient and modified mean bias of the mechanisms for all species measured in the Jernigan et al. (2022) experiment.



## S5 Modelling MSA in the Shen et al. (2022) experiment

40 Understanding the modelling of MSA in the Shen et al. (2022) experiment demonstrates the complexity of MSA formation, and allows an exploration of the uncertainties in the rate constants, and their temperature dependence (due to the experiment being conducted at 263 K). For that experiment, only the Shen mechanism and our mechanism modelled MSA with a fractional gross error of less than 1.5, although the MSA modelled through our mechanism is 3.6 times higher than measured (Figure S13). The MSA from all mechanisms came from the reaction of  $\text{CH}_3\text{SO}_3$  with  $\text{HO}_2$ ; the rate constant for that reaction is

45 an estimate from Yin et al. (1990) and has not been measured experimentally. However, additional uncertainties arise when considering the modelling of  $\text{CH}_3\text{SO}_3$  radicals.

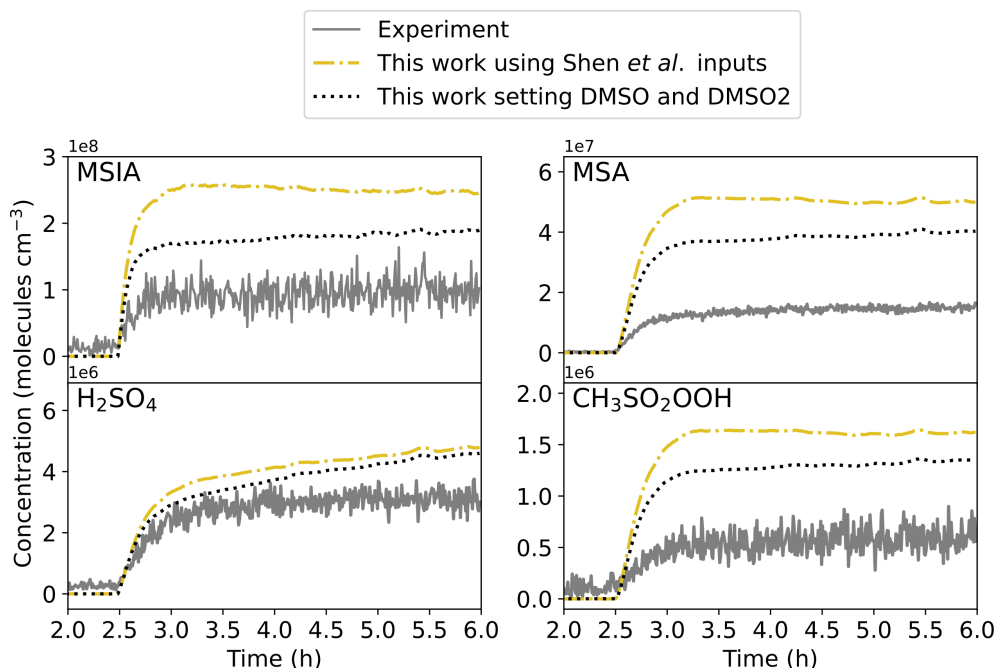


**Figure S13.** The measured MSIA, MSA,  $\text{H}_2\text{SO}_4$  and  $\text{CH}_3\text{SO}_2\text{OOH}$  from the Shen et al. (2022) experiment (grey solid line), compared to the modelled results from the mechanism from this study, using the model inputs from the Shen et al. (2022) paper (yellow dot-dashed line), and from setting the DMSO and DMSO2 concentrations to those measured in the experiment (black dotted line).

In the Shen mechanism, and the mechanism developed in this study, the modelled  $\text{CH}_3\text{SO}_3$  came from MSIA reacting with OH radicals; this reaction forms  $\text{CH}_3\text{SO}_2$ , which then typically dissociates to form  $\text{SO}_2$  and  $\text{CH}_3$  or eventually becomes the  $\text{CH}_3\text{SO}_3$  radical (other pathways are possible, but minor). In the other mechanisms, the products of the MSIA reaction with OH are  $\text{SO}_2$  and  $\text{CH}_3$ , which results in less MSA being produced by those mechanisms for this experiment (as no  $\text{CH}_3\text{SO}_3$  forms through MSIA oxidation). There is only one study that measured the reaction between MSIA and OH, Kukui et al. (2003), which found that  $\text{SO}_2$  formed at unit yield. However, that experiment was conducted in the absence of oxygen, which is needed to form  $\text{CH}_3\text{SO}_3$ , and products other than  $\text{SO}_2$ .

50

The mechanism from this work overestimates the MSA formed, which could be due to a few factors. As the MSIA modelled through our mechanism overestimates the experiments (2.6 times higher than measured), it could account for some of the overestimation of MSA in the model. The overestimation of MSA could also indicate that the rate constant used for the reaction between MSIA and OH (by Kukui et al. (2003)) is too fast at this temperature (263 K). Additionally, there are also large uncertainties in the reactions of  $\text{CH}_3\text{SO}_3$  (including the reaction with  $\text{HO}_2$  to form MSA), and the modelled concentration of  $\text{HO}_2$ .

The overestimation of MSIA from the models, formed from the reaction of DMSO with OH, can come from a few sources. The DMSO formed is also overestimated in the mechanisms, which would result in an overestimation of MSIA, however, DMSO (and  $\text{DMSO}_2$ ) formed in the Shen et al. (2022) experiment was found to come from both gas-phase reactions and wall reactions (which were included as part of the auxiliary mechanism). To investigate the formation of MSIA from DMSO, the DMSO and  $\text{DMSO}_2$  were set to the measured values (Figure S13, black dotted lines). Setting the DMSO to the measured values did decrease the MSIA modelled by 28%, however, the model still overestimated MSIA by around 89% compared to the measured MSIA concentration.

The rate constant for the DMSO and OH reaction forming MSIA is well established at 298 K ( $8.9 \times 10^{-11} \text{ cm}^3 \text{ molecules}^{-1} \text{ s}^{-1}$ , Burkholder et al. (2019)), but only one temperature-dependent study was performed (at temperatures above room temperature) which contained large uncertainties. That study by Hynes and Wine (1996) found that the OH reaction with DMSO had a negative activation energy (the rate constant increased with decreasing temperature) where  $E/R = -800 \pm 540 \text{ K}$ . However, to fit the MSIA formed, a rate constant slower than the rate constant determined at 298 K would be needed ( $5.7 \times 10^{-11} \text{ cm}^3 \text{ molecules}^{-1} \text{ s}^{-1}$ ). This indicates that the temperature dependence of this reaction should be studied further.

Further experiments on the reactions of DMSO and MSIA with OH radicals, and their temperature dependence, could improve the modelling of MSA at the lower temperatures studied in the Shen et al. (2022) experiments (263 K). Additionally, experiments to determine the rate of the reaction of  $\text{CH}_3\text{SO}_3$  reaction with  $\text{HO}_2$  could further improve MSA modelling in the marine environment.

## S6 Marine boundary layer

**Table S6.** The initial and background concentrations of species used in the remote marine boundary layer run

Species	Concentration (ppm)
M	$1 \times 10^6$
N <sub>2</sub>	$7.8 \times 10^5$
O <sub>2</sub>	$2.1 \times 10^5$
H <sub>2</sub> O	$1 \times 10^4$
CH <sub>4</sub>	1.8
CO	0.1
H <sub>2</sub>	0.5
O <sub>3</sub>	$3 \times 10^{-2}$
H <sub>2</sub> O <sub>2</sub>	$1 \times 10^{-3}$
NO	$1 \times 10^{-6}$
NO <sub>2</sub>	$1 \times 10^{-5}$
HNO <sub>3</sub>	$5 \times 10^{-4}$
DMS	$2 \times 10^{-4}$
SO <sub>2</sub>	$2 \times 10^{-5}$

**Table S7.** The temperature and planetary boundary layer (PBL) height over the diurnal cycle.

Time (h)	Temperature (K)	PBL height (m)
0	289.5359	1300
1	289.1363	1300
2	289.0000	1350
3	289.1363	1400
4	289.5359	1450
5	290.1716	1500
6	291.0000	1550
7	291.9647	1450
8	293.0000	1400
9	294.0353	1350
10	295.0000	1300
11	295.8284	1250
12	296.4641	1200
13	296.8637	1200
14	297.0000	1200
15	296.8637	1200
16	296.4641	1150
17	295.8284	1150
18	295.0000	1100
19	294.0353	1200
20	293.0000	1300
21	291.9647	1400
22	291.0000	1400
23	290.1716	1350
24	289.5359	1300

**Table S8.** The percentage distribution of the products of DMS oxidation for each mechanism, from the average concentration over two days of the marine boundary layer box model run

Species	Jernigan	Ye	MCM	Shen	This work
SO <sub>2</sub>	63.5	67.1	75.9	33.7	58.4
HPMTF	16.0	20.5	0.0	53.8	9.2
H <sub>2</sub> SO <sub>4</sub>	8.5	9.0	10.1	4.9	9.9
OCS	5.8	0.0	0.0	0.0	9.8
CH <sub>3</sub> SCHO	0.5	0.5	8.5	0.2	0.7
OCHSOH	0.0	0.0	0.0	0.0	5.0
MSIA	1.3	1.4	1.5	4.5	1.1
DMSO <sub>2</sub>	2.9	0.0	0.0	0.2	2.6
CH <sub>3</sub> SCH <sub>2</sub> OOH	0.1	0.1	2.2	0.0	0.2
DMSO	1.4	1.4	1.5	1.0	1.3
TPA	0.0	0.0	0.0	0.0	1.4
MSA	0.0	0.0	0.0	1.2	0.1
HOCH <sub>2</sub> SCH <sub>2</sub> OOH	0.0	0.0	0.0	0.4	0.1
CH <sub>3</sub> SCH <sub>2</sub> OH	0.0	0.0	0.3	0.0	0.0

## References

- Albu, M., Barnes, I., Becker, K. H., Patroescu-Klotz, I., Benter, T., and Mocanu, R.: FT-IR Product Study On The OH Radical Initiated Oxidation Of Dimethyl Sulfide: Temperature And O<sub>2</sub> Partial Pressure Dependence, in: Simulation and Assessment of Chemical Processes in a Multiphase Environment, edited by Barnes, I. and Kharytonov, M. M., pp. 501–513, Springer Science, Dordrecht, [https://doi.org/10.1007/978-1-4020-8846-9\\_41](https://doi.org/10.1007/978-1-4020-8846-9_41), 2008.
- Atkinson, R., Baulch, D. L., Cox, R. A., Crowley, J. N., Hampson, R. F., Hynes, R. G., Jenkin, M. E., Rossi, M. J., and Troe, J.: Evaluated kinetic and photochemical data for atmospheric chemistry: Volume I - gas phase reactions of O<sub>x</sub>, HO<sub>x</sub>, NO<sub>x</sub> and SO<sub>x</sub> species, *Atmos. Chem. Phys.*, 4, 1461–1738, <https://doi.org/10.5194/acp-4-1461-2004>, 2004.
- Berndt, T., Scholz, W., Mentler, B., Fischer, L., Hoffmann, E. H., Tilgner, A., Hyttinen, N., Prisle, N. L., Hansel, A., and Herrmann, H.: Fast Peroxy Radical Isomerization and OH Recycling in the Reaction of OH Radicals with Dimethyl Sulfide, *J. Phys. Chem. Lett.*, 10, 6478–6483, <https://doi.org/10.1021/acs.jpcclett.9b02567>, 2019.
- Berndt, T., Chen, J., Møller, K. H., Hyttinen, N., Prisle, N. L., Tilgner, A., Hoffmann, E. H., Herrmann, H., and Kjaergaard, H. G.: SO<sub>2</sub> formation and peroxy radical isomerization in the atmospheric reaction of OH radicals with dimethyl disulfide, *Chem. Commun.*, 56, 13 634–13 637, <https://doi.org/10.1039/D0CC05783E>, 2020.
- Burkholder, J. B., Sander, S. P., Abbatt, J. P. D., Barker, J. R., Cappa, C., Crouse, J. D., Dibble, T. S., Huie, R. E., Kolb, C. E., Kurylo, M. J., Orkin, V. L., Percival, C. J., Wilmouth, D. M., and Wine, P. H.: Chemical Kinetics and Photochemical Data for Use in Atmospheric Studies, Evaluation No. 19, Tech. rep., JPL Publication 19-5, Jet Propulsion Laboratory, Pasadena, <http://jpldataeval.nasa.gov/>, 2019.
- Hoffmann, E. H., Tilgner, A., Schrödner, R., Bräuer, P., Wolke, R., and Herrmann, H.: An advanced modeling study on the impacts and atmospheric implications of multiphase dimethyl sulfide chemistry, *Proc. Natl. Acad. Sci. U. S. A.*, 113, 11 776–11 781, <https://doi.org/10.1073/pnas.1606320113>, 2016.
- Hynes, A. J. and Wine, P. H.: The atmospheric chemistry of dimethylsulfoxide (DMSO) kinetics and mechanism of the OH+DMSO reaction, *J. Atmos. Chem.*, 24, 23–37, <https://doi.org/10.1007/BF00053821>, 1996.
- Jernigan, C. M., Fite, C. H., Vereecken, L., Berkelhammer, M. B., Rollins, A. W., Rickly, P. S., Novelli, A., Taraborrelli, D., Holmes, C. D., and Bertram, T. H.: Efficient Production of Carbonyl Sulfide in the Low-NO<sub>x</sub> Oxidation of Dimethyl Sulfide, *Geophys. Res. Lett.*, 49, e2021GL096 838, <https://doi.org/https://doi.org/10.1029/2021GL096838>, 2022.
- Kukui, A., Borissenko, D., Laverdet, G., and Le Bras, G.: Gas-Phase Reactions of OH Radicals with Dimethyl Sulfoxide and Methane Sulfinic Acid Using Turbulent Flow Reactor and Chemical Ionization Mass Spectrometry, *J. Phys. Chem. A*, 107, 5732–5742, <https://doi.org/10.1021/jp0276911>, 2003.
- Lucas, D. D. and Prinn, R. G.: Mechanistic studies of dimethylsulfide oxidation products using an observationally constrained model, *J. Geophys. Res.: Atmos.*, 107, ACH 12 1–26, <https://doi.org/https://doi.org/10.1029/2001JD000843>, 2002.
- Sander, S. P., Abbatt, J., Barker, J. R., Burkholder, J. B., Friedl, R. R., Golden, D. M., Huie, R. E., Kolb, C. E., Kurylo, M. J., Moortgat, G. K., Orkin, V. L., and Wine, P. H.: Chemical Kinetics and Photochemical Data for Use in Atmospheric Studies, Evaluation No. 17, Tech. rep., JPL Publication 10-6, Jet Propulsion Laboratory, Pasadena, <http://jpldataeval.nasa.gov/>, 2011.
- Shen, J., Scholz, W., He, X.-C., Zhou, P., Marie, G., Wang, M., Marten, R., Surdu, M., Rörup, B., Baalbaki, R., Amorim, A., Ataei, F., Bell, D. M., Bertozzi, B., Bresseur, Z., Caudillo, L., Chen, D., Chu, B., Dada, L., Duplissy, J., Finkenzeller, H., Granzin, M., Guida, R., Heinritzi, M., Hofbauer, V., Iyer, S., Kempainen, D., Kong, W., Krechmer, J. E., Kürten, A., Lamkaddam, H., Lee, C. P., Lopez, B., Mahfouz, N. G. A., Manninen, H. E., Massabò, D., Mauldin, R. L., Mentler, B., Müller, T., Pfeifer, J., Philippov, M., Piedadhierro,

- 115 A. A., Roldin, P., Schobesberger, S., Simon, M., Stolzenburg, D., Tham, Y. J., Tomé, A., Umo, N. S., Wang, D., Wang, Y., Weber, S. K., Welti, A., Wollesen de Jonge, R., Wu, Y., Zauner-Wieczorek, M., Zust, F., Baltensperger, U., Curtius, J., Flagan, R. C., Hansel, A., Möhler, O., Petäjä, T., Volkamer, R., Kulmala, M., Lehtipalo, K., Rissanen, M., Kirkby, J., El-Haddad, I., Bianchi, F., Sipilä, M., Donahue, N. M., and Worsnop, D. R.: High Gas-Phase Methanesulfonic Acid Production in the OH-Initiated Oxidation of Dimethyl Sulfide at Low Temperatures, *Environ. Sci. Technol.*, 56, 13 931–13 944, <https://doi.org/10.1021/acs.est.2c05154>, 2022.
- 120 Veres, P. R., Neuman, J. A., Bertram, T. H., Assaf, E., Wolfe, G. M., Williamson, C. J., Weinzierl, B., Tilmes, S., Thompson, C. R., Thames, A. B., Schroder, J. C., Saiz-Lopez, A., Rollins, A. W., Roberts, J. M., Price, D., Peischl, J., Nault, B. A., Møller, K. H., Miller, D. O., Meinardi, S., Li, Q., Lamarque, J.-F., Kupc, A., Kjaergaard, H. G., Kinnison, D., Jimenez, J. L., Jernigan, C. M., Hornbrook, R. S., Hills, A., Dollner, M., Day, D. A., Cuevas, C. A., Campuzano-Jost, P., Burkholder, J., Bui, T. P., Brune, W. H., Brown, S. S., Brock, C. A., Bourgeois, I., Blake, D. R., Apel, E. C., and Ryerson, T. B.: Global airborne sampling reveals a previously unobserved dimethyl sulfide oxidation mechanism in the marine atmosphere, *Proc. Natl. Acad. Sci. U. S. A.*, 117, 4505–4510, <https://doi.org/10.1073/pnas.1919344117>, 2020.
- 125 Vermeuel, M. P., Novak, G. A., Jernigan, C. M., and Bertram, T. H.: Diel Profile of Hydroperoxymethyl Thioformate: Evidence for Surface Deposition and Multiphase Chemistry, *Environ. Sci. Technol.*, 54, 12 521–12 529, <https://doi.org/10.1021/acs.est.0c04323>, 2020.
- Wu, R., Wang, S., and Wang, L.: New Mechanism for the Atmospheric Oxidation of Dimethyl Sulfide. The Importance of Intramolecular Hydrogen Shift in a  $\text{CH}_3\text{SCH}_2\text{OO}$  Radical, *J. Phys. Chem. A*, 119, 112–117, <https://doi.org/10.1021/jp511616j>, 2015.
- 130 Ye, Q., Goss, M. B., Isaacman-VanWertz, G., Zaytsev, A., Massoli, P., Lim, C., Croteau, P., Canagaratna, M., Knopf, D. A., Keutsch, F. N., Heald, C. L., and Kroll, J. H.: Organic Sulfur Products and Peroxy Radical Isomerization in the OH Oxidation of Dimethyl Sulfide, *ACS Earth Space Chem.*, 5, 2013–2020, <https://doi.org/10.1021/acsearthspacechem.1c00108>, 2021.
- Ye, Q., Goss, M. B., Krechmer, J. E., Majluf, F., Zaytsev, A., Li, Y., Roscioli, J. R., Canagaratna, M., Keutsch, F. N., Heald, C. L., and Kroll, J. H.: Product distribution, kinetics, and aerosol formation from the OH oxidation of dimethyl sulfide under different  $\text{RO}_2$  regimes, *Atmos. Chem. Phys.*, 22, 16 003–16 015, <https://doi.org/10.5194/acp-22-16003-2022>, 2022.
- 135 Yin, F., Grosjean, D., and Seinfeld, J. H.: Photooxidation of dimethyl sulfide and dimethyl disulfide. I: Mechanism development, *J. Atmos. Chem.*, 11, 309–364, <https://doi.org/10.1007/BF00053780>, 1990.